SCIENTIFIC REPORTS

OPEN

SUBJECT AREAS:
X-RAY CRYSTALLOGRAPHY
ION TRANSPORT
METALLOPROTEINS
BIOPHYSICAL CHEMISTRY

Received
10 September 2012

Accepted
26 November 2012

Published
19 December 2012

Correspondence and requests for materials should be addressed to H.S. (hsun@hku.hk)

Iron and bismuth bound human serum transferrin reveals a partially-opened conformation in the N-lobe

Nan Yang[1,2], Hongmin Zhang[3], Minji Wang[1], Quan Hao[3] & Hongzhe Sun[1]

[1]Department of Chemistry, the University of Hong Kong, Pokfulam Road, Hong Kong, P.R. China, [2]Department of Physiology, Johns Hopkins University, Baltimore, Maryland, USA, [3]Department of Physiology, the University of Hong Kong, Sassoon Road, Hong Kong, P.R. China.

Human serum transferrin (hTF) binds Fe(III) tightly but reversibly, and delivers it to cells via a receptor-mediated endocytosis process. The metal-binding and release result in significant conformational changes of the protein. Here, we report the crystal structures of diferric-hTF (Fe_NFe_C-hTF) and bismuth-bound hTF (Bi_NFe_C-hTF) at 2.8 and 2.4 Å resolutions respectively. Notably, the N-lobes of both structures exhibit unique "partially-opened" conformations between those of the apo-hTF and holo-hTF. Fe(III) and Bi(III) in the N-lobe coordinate to, besides anions, only two (Tyr95 and Tyr188) and one (Tyr188) tyrosine residues, respectively, in contrast to four residues in the holo-hTF. The C-lobe of both structures are fully closed with iron coordinating to four residues and a carbonate. The structures of hTF observed here represent key conformers captured in the dynamic nature of the transferrin family proteins and provide a structural basis for understanding the mechanism of metal uptake and release in transferrin families.

Iron is essential for virtually all types of cells and organisms. However, too much iron is lethal[1]. Therefore, it is necessary to precisely regulate intracellular iron homeostasis and transport the metal to diverse locations and subsequently insert it into the correct proteins and metalloenzymes[2]. Transferrin (TF) family proteins, non-heme iron-transport glycoproteins with molecular weights of *ca.* 80 kDa, are found in multicellular organisms from cockroaches to humans, playing the role of carrying iron (Fe(III)) from the sites of intake to the circulation system, and to the cells and tissues[3]. Three major types of transferrins (serum TF, ovotransferrin and lactoferrin) and one transferrin superfamily (ferric ion-binding protein, fbp) have been characterized[4–6]. Human serum transferrin (hTF), a member of the sub-family of serum TF, mainly synthesized by hepatocytes[3,4], tightly but reversibly binds iron (K_d of $\sim 10^{-22}$ M)[7] and transports it from extracellular fluid to cytosol, thereby playing a critical role in the maintenance of human cellular iron homeostasis[8,9] as well as the prevention of damage from free radicals[10,11]. Deficiencies in human transferrin lead to insufficient cellular iron, which subsequently inhibits cell growth and proliferation[12]. Moreover, human transferrin is rich in blood plasma (2.5 mg/ml) with only 30% saturation of Fe(III), the protein has therefore been regarded as a "vehicle" to transport therapeutic (Bi(III)), radio diagnostic (^{67}Ga(III) and ^{111}In(III)) and toxic (Al(III) and Pu(IV)) metals in biological systems[4,13,14]. As revealed previously, these metal ions share the similar coordination sites to Fe(III) in TF proteins, locating in the binding clefts formed within the protein's two homologous halves (N- and C-lobe).

It has been well established that hTF transports metal via a hTF receptor (TfR)-mediated endocytosis process[5,15,16], and the tertiary structure of hTF is crucial for its recognition by transferrin receptor[13]. The alteration of the tertiary structure of hTF is accompanied by metal binding and release[13,17], i.e. hTF occludes the lobe cleft upon metal binding, and opens up upon metal dissociation[4,18,19]. Such a metal triggered conformational change is also essential in hTF's biological turnover[13,18,20,21] because TfR exhibits a higher binding affinity to diferric bound hTF (holo-hTF) than the nonferric bound form (apo-hTF) in the extracellular region (pH $\approx$ 7.5), leading to the subsequent internalization of iron bound hTF and release of apo-hTF on cell surface. While in the endosome (pH $\approx$ 5.6), the binding of TfR to apo-hTF is preferential to holo-hTF, resulting in the trafficking of apo-hTF from endosome to extracellular membrane with TfR[8]. In such a process, iron is delivered into the cells and hTF is recycled.

The constant motion of proteins has been known to be important to maintain their specific biological functions[22,23]. However, it is not clear how TF proteins undergo conformational changes upon metal binding and

dissociation due to the lack of structural data of intermediate conformers. In fact, all available structures of TF proteins assume two polar conformations: either a "fully-opened" conformation for apo-TF such as the resolved crystal structure of apo-hTF or a "fully-closed" conformation for holo-TF such as the resolved structure of the truncated iron bound N-lobe of hTF (Fe-hTF/2N)[2]. There is no structure available in that the TF proteins exhibit an in-between state adopting a "partially-opened" conformation, though such a structure is extremely important for the study of their conformational change. To this end, we report the crystal structures of diferric hTF (Fe_NFe_C-hTF) and bismuth bound hTF (Bi_NFe_C-hTF). Notably, for the first time, the two hTF structures exhibit unique "partially-opened" conformations in the N-lobe with diverse opening extent, representing two essential protein conformers during the metal release process. Equally important, the structure of Bi_NFe_C-hTF provides the direct information on Bi(III) coordination, offering a structural basis for the potential role of transferrin as a metallodrug delivery "vehicle" in healthcare[4,14].

Results

Overall structures of Fe_NFe_C-hTF and Bi_NFe_C-hTF. The crystals of Fe_NFe_C-hTF and Bi_NFe_C-hTF were obtained at pH 7.4 and the structures were solved to a resolution of 2.8 and 2.4 Å respectively by the molecular replacement method (Table 1). Similar to other members in transferrin superfamily, the overall structures of the Fe_NFe_C-hTF and Bi_NFe_C-hTF show the bilobal nature of the molecule with two homologous halves (*ca.* 44% sequence identity), termed N-lobe (residues 1–330) and C-lobe (340–679) and can be further divided into N1- (1–92 and 247–330), N2- (93–246), C1- (340–425 and 573–679) and C2-subdomains (426–572), Figure 1a. The N-lobe contains 14 helices and 13 strands whereas the C-lobe is composed of 17 helices and 13 strands (Figure S1). The tertiary structure of the protein is stabilized by intra-/inter-lobe interactions and an unstructured peptide linker (331–339) (Figure S2)[24,25]. Each lobe of the Fe_NFe_C-hTF houses a Fe(III) in its specific iron binding site, which is located at the bottom of lobe-cleft formed by folding of the two respective subdomains (Figure 1a). For Bi_NFe_C-hTF, anomalous electron density map, contoured at 10 σ, shows density only in the N-lobe of hTF (Figure 1d and Figure S3), unambiguously demonstrating that Bi(III) is only located in the metal binding cleft of the N-lobe. The two subdomains (C1- and C2-subdomains) of the C-lobe in both structures of Fe_NFe_C-hTF and Bi_NFe_C-hTF are involved in Fe(III) coordination, conforming to the fold that is characteristic of the members in the transferrin superfamily (Figure 1c and Figure S3), i.e. the C-lobe in both structures exhibits a "fully-closed" conformation, similar to other iron bound transferrin families. However, the N-lobe in both

Table 1 | Data collection and refinement statistics of Fe_NFe_C-hTF and Bi_NFe_C-hTF

Protein	Fe_NFe_C-hTF	Bi_NFe_C-hTF
Data collection		
Wavelength (Å)	0.97924	0.92000
Space group	$P2_12_12_1$	$P2_12_12_1$
Cell dimensions		
a, *b*, *c* (Å)	73.845, 90.435, 112.299	73.907, 90.165, 111.032
α, β, γ (°)	90.00, 90.00, 90.00	90.00, 90.00, 90.00
Resolution (Å)	50~2.8 (2.90~2.80)*	50~2.4 (2.49~2.40)
R_{sym} or R_{merge} (%)	10.6 (52.4)	8.2 (59.7)
$I/\sigma I$	17.3 (1.6)	26.0 (3.5)
Completeness (%)	92.9 (77.4)	99.6 (100)
Redundancy	5.5 (2.6)	7.0 (7.3)
Refinement		
Resolution (Å)	50~2.80	50~2.40
No. reflections	16769	27755
R_{work}/R_{free}	0.2062 / 0.2757	0.1941 / 0.2560
No. atoms		
Protein	5265**	5266
Fe/CO_3/NAG/SO_4	2/8/28/5	1/1/8/14/13
Water	9	130
Average *B* factor (Å^2)	21.8	19.0
R.m.s. deviations		
Bond lengths (Å)	0.008	0.008
Bond angles (°)	1.15	1.12
Ramachandranplot (%)		
Most favored regions	83.2	88.8
Additionally allowed	15.6	10.2
Generously allowed	0.7	0.3
Disallowed regions	0.5	0.7

*Values in parentheses are for the highest-resolution shell.
**The deposited structure of Fe_NFe_C-hTF was built up based on the sequence of apo-hTF (PDB: 2HAV).

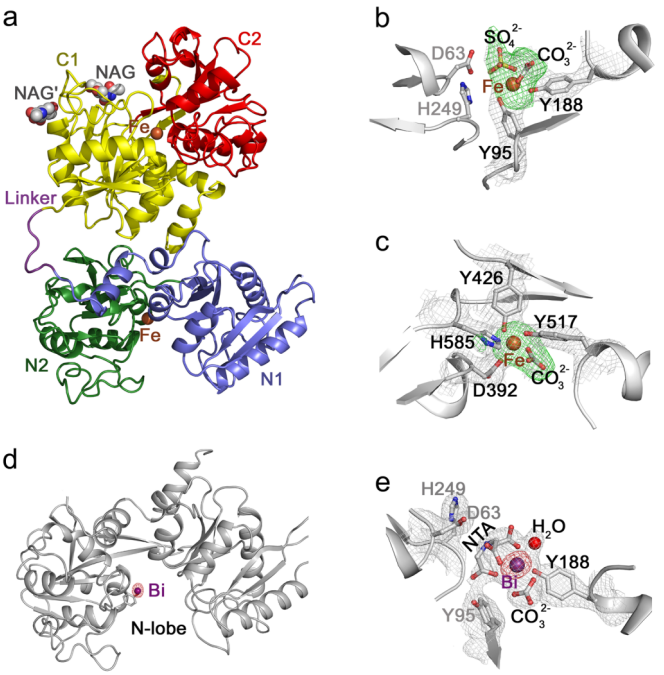

Figure 1 | (a) Ribbon representation of the overall structure of Fe_NFe_C-hTF with subdomains N1 in blue, N2 in green, C1 in yellow, C2 in red, and peptide linker in purple. Fe(III) ions are represented as sphere models in brown. The two N-acetylglucosamine moieties (NAG and NAG'), represented as sphere models. (b) Coordination of the Fe(III) in the N-lobe of Fe_NFe_C-hTF. The gray $2F_{obs}$-F_{calc} map is contoured at 1.0 σ and the green F_{obs}-F_{calc} map (computed before the Fe(III), CO_3^{2-} and SO_4^{2-} were modeled) is contoured at 3.0 σ. The carboxyl group of Asp63 and imidazole group of His249 are *ca.* 7 and 10 Å away from the Fe(III). (c) Iron binding center in the C-lobe of Fe_NFe_C-hTF. The gray $2F_{obs}$-F_{calc} map is contoured at 1.0 σ and the green F_{obs}-F_{calc} map (computed before the Fe(III) and CO_3^{2-} were modeled) is contoured at 3.0 σ. (d) Anomalous electron density of Bi_NFe_C-hTF. The hTF backbone is shown in gray ribbon with the residue Tyr188 and Bi(III) represented as stick and sphere models respectively. The anomalous electron density map (contoured at 10 σ), calculated from diffraction data collected at 0.92000 Å, is shown as red mesh and indicates the location of atoms that strongly absorb X-ray photons of this energy. (e) Coordination of Bi(III) in the N-lobe of Bi_NFe_C-hTF. The gray $2F_{obs}$-F_{calc} map is contoured at 1.0 σ and the red anomalous electron map is contoured at 10.0 σ. The side chains of putative binding residues Asp63, Tyr95 and His249 are 6.7, 9.9 and 5.5 Å away from the Bi(III), respectively.

structures adopts unique tertiary structures with their lobe-cleft partially opened, different to either reported apo-TF or metal bound TF proteins (*vide infra*).

Furthermore, electron densities are observed in the vicinity of residues Asn413 and Asn611 in the C-lobe of Fe_NFe_C-hTF, indicative of the connection of two glycan moieties (NAG, N-acetylglucosamine) to these residues (Figure 1a and Figure S4). Although insufficient electron densities precluded the molecular replacement of entire glycan chains in the model, the first connected glycan moiety can be readily identified in the structure of Fe_NFe_C-hTF.

Metal coordination in the N-lobe of Fe_NFe_C-hTF and Bi_NFe_C-hTF. Only two tyrosine residues (Tyr95 and Tyr188) in the N2-subdomain as protein ligands are involved in iron coordination in the N-lobe of Fe_NFe_C-hTF (Figure 1b and Table 2), whereas Bi(III) is anchored by only one tyrosine residue (Tyr188) in the N-lobe of Bi_NFe_C-hTF (Figure 1e and Table 2). The two putative binding residues (Asp63 and His249) which are conserved in all TF proteins in the N1-subdomain (Figure S5), are shifted away from the metal coordination sites in both structures. They are *ca.* 7 and 10 Å away from the Fe(III) in Fe_NFe_C-hTF and 6.7 and 10 Å away from the Bi(III) in Bi_NFe_C-hTF, respectively. In the structure of Bi_NFe_C-hTF, the distance between Bi(III) and the phenol group of Tyr95 is *ca.* 5.5 Å. A bidentate carbonate (as a synergistic anion) coordinates to the metal and is stabilized by interaction with Arg124 in both structures. Besides the above binding ligands that are commonly subsistent in metal bound TF proteins, there are extra signals in the F_{obs}-F_{calc} electron density map adjacent to the carbonate in both structures of Fe_NFe_C-hTF and Bi_NFe_C-hTF (Figure 1b). Given the fitting of the electron density map and the use of $NH_4Fe(SO_4)_2$ and bismuth nitrilotriacetate (Bi(NTA)) in the preparations of Fe_NFe_C-hTF and Bi_NFe_C-hTF, a bidentate sulfate (SO_4^{2-}) and a tridentate nitrilotriacetate (NTA) as an additional coordination anion is modeled in the structures of Fe_NFe_C-hTF and Bi_NFe_C-hTF, respectively (Figure 1b and 1e).

Conformational changes in the N-lobe of hTF. It has long been believed that the uptake and release of metal ions by hTF are pH dependent processes and accompanied with the transposition of lobe opening and closure, i.e. from "fully-opened" to "fully-closed" state upon iron binding at extracellular pH (pH ≈ 7.5), and from "fully-closed" to "fully-opened" conformation upon iron release at endosomal pH (pH ≈ 5.6)[2,4]. To our surprise, despite the fact that the diferric and mono-bismuth bound forms of hTF in this report were prepared and crystallized at pH = 7.4, their N-lobes adopt a unique "partially-opened" conformation, different from either the apo-hTF with a "fully-opened" conformation[26] or the isolated iron bound recombinant N-lobe of hTF (Fe-hTF/2N) and a recently reported diferric hTF with a "fully-closed" conformation[25,27,28].

Besides carbonate (CO_3^{2-}), an additional ligand (modeled as SO_4^{2-} in Fe_NFe_C-hTF and NTA in Bi_NFe_C-hTF) partially occupies the metal binding sites and prevents the coordination of other putative residues to metal ions. As shown in Figure 2a, when the N2-subdomains of the apo-hTF, Fe_NFe_C-hTF, Bi_NFe_C-hTF and Fe-hTF/2N are superimposed (shown as Cα), the relative opening extent of the cleft in the N-lobe is readily visualized by the shifts of beta-strand 3 (β_3) in the N1-subdomain due to its direct connecting to the residue Asp63, a conserved putative metal binding residue in all TF proteins (Figure S5). The β_3 and residue Asp63 of Fe_NFe_C-hTF and Bi_NFe_C-hTF are located between those in apo-hTF and Fe-hTF/2N, clearly illustrating the relative twist motion of subdomains in the N-lobe during the metal release process. Similar positional shifts can also be observed when other motifs such as α_1, β_1, β_{11} and another conserved putative binding residue His249 in N1-subdomain are tracked (Figure 2b and Figure S6). Moreover, the conformations of the N-lobe of the current structures are not only unique from the reported hTF structures, but also unparalleled among all the transferrin superfamilies, exhibiting an intermediate feature when compared to the iron bound or apo forms of ovotransferrin of hen and duck; lactoferrins (LFs) of human and bovine, and serum transferrins of rabbit, porcine and bovine (Table 3).

For transferrin proteins, the extent to which each lobe is opened can be quantified by superimposing one subdomain of the protein with the corresponding subdomain of the known structure (of a TF protein with "opened" or "closed" conformation) and examining the rotation and translation functions required to overlap another subdomain[29]. Based on the known structures of apo-hTF and Fe-hTF/2N and by using the program Superpose from CCP4 suite[30], the opening extent of the N-lobe in Fe_NFe_C-hTF and Bi_NFe_C-hTF are precisely evaluated. As shown in Figure 2c and Table 3, when the N2-subdomains of these proteins are superimposed, rotations of 48.9° and 56.3° are required to overlap the N1-subdomain of Fe_NFe_C-hTF and Bi_NFe_C-hTF to that of Fe-hTF/2N respectively, while –13.7° and −7.8° are required to overlap with the apo-hTF, clearly demonstrating that the N-lobe of the current structures adopt a "partially-opened" conformations. Therefore, the structures of Fe_NFe_C-hTF and Bi_NFe_C-hTF represent two intermediate conformers of TF family proteins during their structural change between the two polar conformations. Furthermore, the N-lobe of Fe_NFe_C-hTF and Bi_NFe_C-hTF bear more resemblance to that of the apo-TF with "fully-opened" conformation than to "fully-closed" holo forms[27,31–35]. This is further evidenced by the "dilysine-trigger" (Lys206 and Lys296) which is hydrogen bonded in the "fully-closed" Fe-hTF/2N and far apart in the apo-hTF[36], but is separated by *ca.* 10 and 6 Å away in the structures of Fe_NFe_C-hTF and Bi_NFe_C-hTF, respectively (Figure S7). In the lateral comparison, the opening extent of the N-lobe in Bi_NFe_C-hTF is slightly larger than that of Fe_NFe_C-hTF (Figure 2c and Table 3), in consistence with the metal coordination circumstance, i.e. two tyrosine residues (Tyr95 and Tyr188) are involved in metal coordination in the N-lobe of Fe_NFe_C-hTF whereas only one (Tyr188) is involved in coordination in Bi_NFe_C-hTF.

Interlobe communication in Fe_NFe_C-hTF and Bi_NFe_C-hTF. The tertiary structure of hTF is also affected by the interlobe interactions. As the two separated iron binding domains, the N- and C-lobes of hTF are linked by a peptide (C^{331}PEAPTNEC^{339}), where two disulfide

Table 2 | Bond lengths (Å) of Fe(III) and Bi(III) to coordinated ligands in Fe_NFe_C-hTF and Bi_NFe_C-hTF

Structure	Bond	N-lobe	C-lobe
Fe_NFe_C-hTF	Fe−O Tyr95 (Tyr426)[a]	2.0	1.9
	Fe−O Tyr188 (Tyr517)	1.9	1.9
	Fe−O (Asp392)	–	2.1
	Fe−N (His585)	–	2.1
	Fe−O^2 CO_3^{2-} (CO_3^{2-})	2.6	2.4
	Fe−O^3 CO_3^{2-} (CO_3^{2-})	2.3	2.1
	Fe−O^1 SO_4^{2-}	1.9	–
	Fe−O^3 SO_4^{2-}	2.4	–
Bi_NFe_C-hTF	Bi−O Tyr188	2.4	–
	Bi−O^2 CO_3^{2-}	2.9	–
	Bi−O^3 CO_3^{2-}	2.6	–
	Bi−O^4 NTA	2.4	–
	Bi−O^8 NTA	3.1	–
	Bi−O^{13} NTA	2.4	–
	Bi−O H_2O	2.6	–
	Fe−O Asp392	–	2.1
	Fe−O Tyr426	–	2.0
	Fe−O Tyr517	–	1.9
	Fe−N His585	–	2.3
	Fe−O^2 CO_3^{2-}	–	2.3
	Fe−O^3 CO_3^{2-}	–	2.0

[a]Coordination ligands in the C-lobe are shown in parentheses.

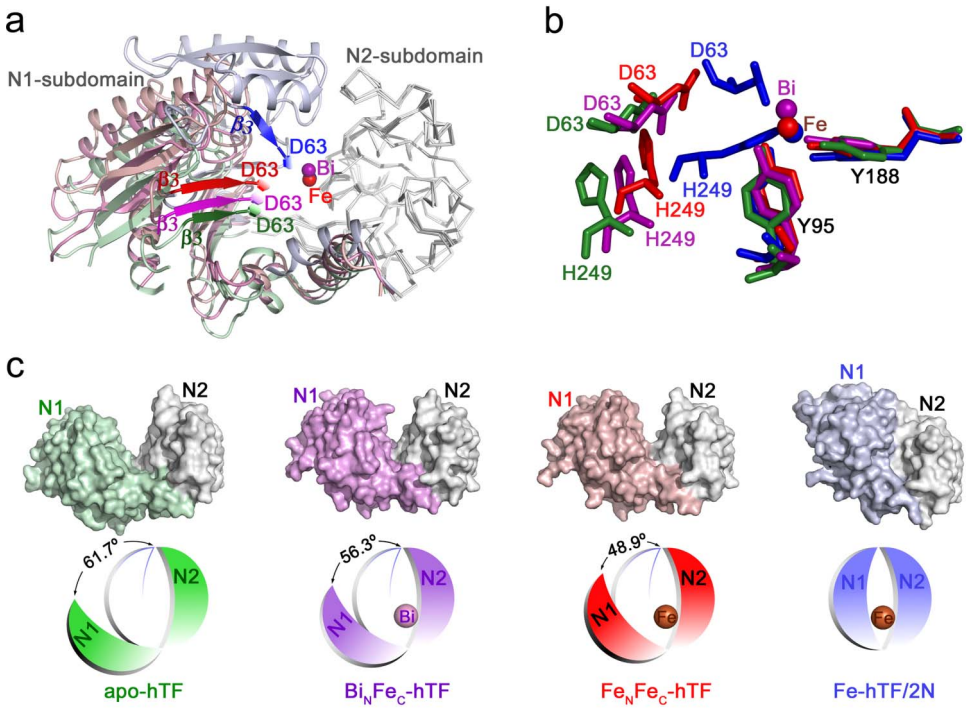

Figure 2 | (a) Superimposition of the N-lobe of Fe-hTF/2N ("fully-closed" conformation), Fe_NFe_C-hTF ("partially-opened" conformation), Bi_NFe_C-hTF ("partially-opened" conformation) and apo-hTF ("fully-opened" conformation). The N2-subdomains of the four proteins are superimposed and represented as Cα in gray, while the N1-subdomains are shown as ribbon models with apo-hTF in pale green, Fe_NFe_C-hTF in salmon, Bi_NFe_C-hTF in purple and Fe-hTF/2N in light blue. Strands β_3 that directly connect to residues Asp63 (hexagonal prism) are highlighted in darker color in each structure. Fe(III) ions are shown as red and blue spheres in Fe_NFe_C-hTF and Fe-hTF/2N, respectively. Bi(III) is shown as purple sphere in Bi_NFe_C-hTF. (b) Position shifts of the key residues in the metal binding center of the N-lobe upon metal binding and dissociation. Coordination residues in Fe-hTF/2N are shown as stick models in blue, while the corresponding residues in Fe_NFe_C-hTF, Bi_NFe_C-hTF and apo-hTF are shown as stick models in red, purple and green, respectively. (c) Molecular surface presentations of the N-lobes in apo-hTF, Bi_NFe_C-hTF, Fe_NFe_C-hTF and Fe-hTF/2N. A schematic diagram shows the opening extent of N-lobe in the structures of Fe_NFe_C-hTF (red), Bi_NFe_C-hTF (purple) and apo-hTF (green) relative to the Fe-hTF/2N (blue).

bonds are formed (Cys331-Cys137 and Cys339-Cys596) (Figure S2). Different from the α-helical structure in human and bovine LFs[37], the linker peptide in hTF exhibits an unstructured feature, conferring flexibility to the protein molecule. Other non-covalent interlobe interactions in hTF, including the salt bridges and hydrogen bonds, are particularly noteworthy. A salt bridge Arg308-Asp376 is observed in Fe_NFe_C-hTF, Bi_NFe_C-hTF and apo-hTF as well as the recently published structure of holo-hTF[28], indicative of its potential role in maintaining the relative immobilization between the N1- and C1-subdomains upon metal binding or release. Another salt bridge between Lys312-Glu385 is observed in the structures of Fe_NFe_C-hTF and holo-hTF but absent in Bi_NFe_C-hTF and apo-hTF, suggesting its potential relevance to the recognition of diferric hTF by TfR, since Glu385 is determined to be a hot interaction spot in the hTF-TfR complex model[38]. The insertion of the C-terminal α-helix (α_{31}) into the N-lobe of hTF is observed in both structures of Fe_NFe_C-hTF and Bi_NFe_C-hTF, proving structural evidence for previous hypothesis that terminal α-helix plays an important role in the interlobe communication (*vide infra*)[15,32]. Furthermore, in the structure of Bi_NFe_C-hTF, a H-bond network was formed through several water molecules located in the interface between the N- and C-lobes. In this water network, side chain and backbone oxygen and nitrogen of residues from the N-lobe (Tyr96, Gln245, Pro307, Arg308, Asp310, Met313, Tyr314, Leu315 and Tyr317) and the C-lobe (Ala379, Met382, Glu672, Arg677 and Arg678) engage in hydrogen bonds with water molecules (Figure S8).

C-terminal helix (α_{31}). Since the orientation of the first half of helix α_{31} (668–678) is fixed by the disulfide bond (Cys674-Cys402), the interactions generated by residues 675 to 678 in both structures of

Table 3 | Comparison of the extent of opening of the cleft in the N-lobe of Fe_NFe_C-hTF, Bi_NFe_C-hTF with transferrin family proteins (as degree (°))[a]

	apo-hTF	Fe-hTF/2N	apo-TF (hen)	Fe_2-TF (hen)	apo-TF (duck)	Fe_2-TF (duck)	apo-LF (human)	Fe_2-LF (human)	Fe_2-TF (rabbit)	Fe_2-TF (porcine)	Fe_2-LF (bovine)
Fe_NFe_C-hTF	−13.7[b]	48.9	−14.4	47.0	−12.9	46.7	−13.2	40.8	49.2	50.1	45.4
Bi_NFe_C-hTF	−7.8	56.3	−14.1	53.8°	−12.7	53.7	−8.4	47.6	56.2	56.9	52.3

[a]The N2-subdomains of Fe_NFe_C-hTF and Bi_NFe_C-hTF are superimposed to apo-hTF (PDB ID: 2HAV), Fe-hTF/2N (PDB ID: 1N84), apo-hen ovotransferrin (apo-TF (hen), PDB ID: 1AIV), diferric hen ovotransferrin (Fe_2-TF (hen), PDB ID: 1OVT), apo-duck ovotransferrin (apo-TF (duck), PDB ID: 1AOV), ferric duck ovotransferrin (Fe_2-TF (duck), PDB ID: 1DOT), apo-human lactoferrin (apo-LF (human), PDB ID: 1CB6), ferric human lactoferrin (Fe_2-LF (human), PDB ID: 1BKA), ferric rabbit transferrin (Fe_2-TF (rabbit), PDB ID: 1JNF), ferric porcine transferrin (Fe_2-TF (porcine), PDB ID: 1H76) and ferric bovine lactoferrin (Fe_2-LF (bovine), PDB ID: 1BLF), respectively. The relative opening extent of Fe_NFe_C-hTF and Bi_NFe_C-hTF to these proteins can be obtained by examining the rotation and translation functions required to overlap the N1-subdomains.
[b]Comparing to the holo-TF and holo-LF, the relative opening extents of Fe_NFe_C-hTF and Bi_NFe_C-hTF to the apo-TF and apo-LF are defined as negative values because their N1-subdomains rotate in an opposite direction.

Fe_NFe_C-hTF and Bi_NFe_C-hTF are particularly examined. In the crystal structure of Fe_NFe_C-hTF, the NH1 group of residue Arg677 engages in hydrogen bonds with the backbone oxygen of Tyr314, Leu315 and Gln245, and its backbone oxygen forms a hydrogen bond with the OE1 group of Gln245. The NH2 group of residue Arg678 engages in hydrogen bonds with the backbone nitrogen of Thr93 and backbone oxygen of Pro91, and its NH1 group forms hydrogen bond with the OE1 group of Gln92 (Figure 3a). In the crystal structure of Bi_NFe_C-hTF, the NH1 group of Arg677 forms a hydrogen bond with the backbone oxygen of residue Tyr314 and a water molecule which engages in hydrogen bonds with the backbone oxygen of residues Leu315 and Gln245. Similar to Fe_NFe_C-hTF, the hydrogen bond between the backbone oxygen of Arg677 and OE1 group of Gln245 is also observed in Bi_NFe_C-hTF. The NH2 group of Arg678 forms a hydrogen bond with the backbone oxygen of residue Lys239 and a water molecule which engages in hydrogen bonds with the NE2 group of Asn245 and OH group of Tyr96. The NH1 group of Arg678 forms salt bridge with OD1 group of Asp240 (Figure 3b). In addition to the above hydrogen bonds and salt bridges, the phenyl group of Phe676 in both structures of Fe_NFe_C-hTF and Bi_NFe_C-hTF are inserted into a N-lobe hydrophobic pocket consisting of residues Ala82, Phe94, Leu303, Val305, Pro306 and Met309 (Figure S9).

Interestingly, comparing to the structures of apo-hTF and Bi_NFe_C-hTF, the guanidinium group of Arg678 from the terminal helix (α_{31}) in Fe_NFe_C-hTF undergoes a rotation of *ca.* 110° to form a hydrogen bond with residue Gln92 from the N1-subdomain; whereas in the structures of apo-hTF and Bi_NFe_C-hTF, Arg678 forms a salt bridge with Asp240 from the N2-subdomain (Figure 4). Since residue Gln92 is located very close to the metal binding residue Tyr95, the non-covalent interactions between residue Gln92 and the C-terminal helix (α_{31}) may affect the metal binding and regulate the subdomain motions in the N-lobe of hTF.

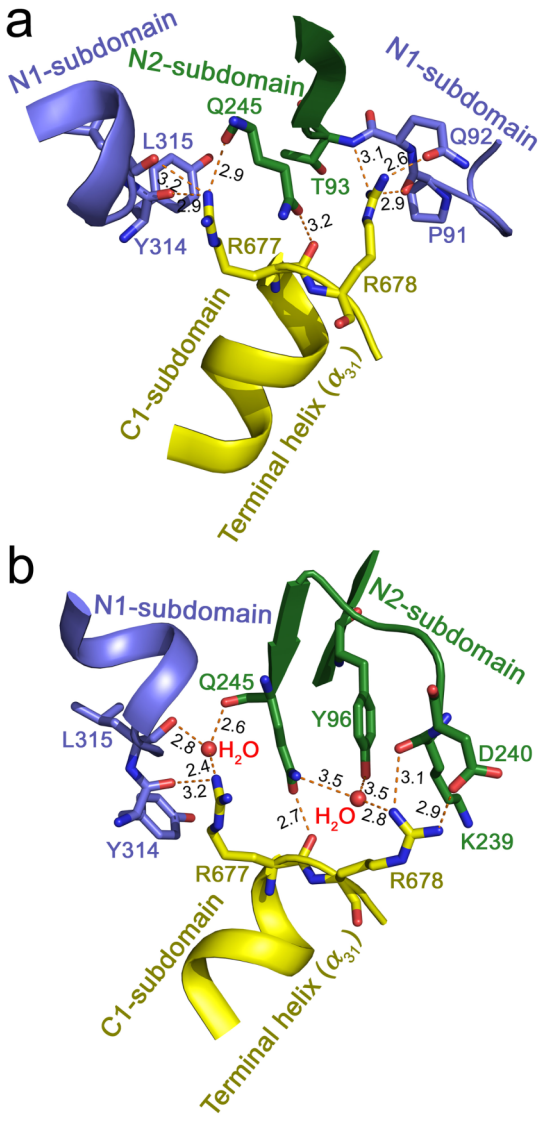

Figure 3 | (a) Interactions between the terminal helix (α_{31}) and residues of N-lobe in Fe_NFe_C-hTF. (b) Interactions between the terminal helix (α_{31}) and residues of N-lobe in Bi_NFe_C-hTF. The interaction residues are represented in stick model with color corresponding to different subdomains as shown in Figure 1a. The water molecules are shown in red as sphere model.

Discussion

Iron is essential for many biological processes and there are a variety of specialized systems for transport, uptake and storage of the metal. The major mode of iron transfer through the body is via the transferrin. Transferrin (hTF) binds ferric ion (Fe(III)) tightly but reversibly, and delivers the metal to cells via a receptor-mediated endocytosis[2,4]. Iron binding and release result in significant conformational changes of the protein, which is crucial for the recognition by its receptor. However, the molecular mechanism of iron uptake and release accompanied by protein conformational changes is not fully understood.

We report the first crystal structures of intact diferric and bismuth bound hTF, and importantly found that the protein exhibits unique "partially-opened" conformations in their N-lobes (Figure 2), unveiling two important protein conformers in the metal release process. The direct observation of such "partially-opened" conformers in the N-lobe of hTF clearly provides a series of snapshots of the dynamic motion of subdomains upon metal (such as Fe(III), Ga(III) and Bi(III))[39] binding and dissociation, not only offering a structural basis for metal uptake and release for transferrin family proteins, but also implicating a common feature for proteins and enzymes in motion. The observation of such a unique conformation is also in agreement with a previously proposed "intermediate" of transferrin based on X-ray absorption fine structure (XAFS) spectroscopy and X-ray solution scattering together with mutant variants and binding of different metal ions[40,41]. The first crystal structure of Bi(III) bound biomolecule (Bi_NFe_C-hTF) offers a good starting point to further

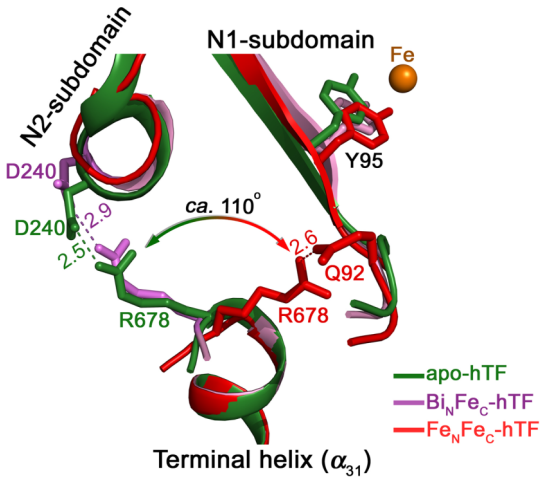

Figure 4 | **Superimposition of Fe_NFe_C-hTF (red) and Bi_NFe_C-hTF (purple) onto apo-hTF (green) shows the rotation of residue Arg678.** The superimposition was made based on the N1- and C1-subdomains (residues 340–425 and 573–679) of the three protein structures.

examine the potential role of transferrin as a delivery "vehicle" for metallodrugs, in view of unsaturated iron binding characteristic of transferrin, i.e. only 30% saturated with iron in blood plasma. Human transferrin was found to bind bismuth and probably serves as a target of the metallodrug in blood plasma[39,42,43].

The C-lobe of the metal bound protein adopts a closed structure, almost identical to reported transferrin families[2]. The conformational differences in the C- and N-lobes of human transferrin (Fe_2-hTF) indicate a slightly different biological function of the two lobes. The C-lobe of hTF is shown to play a major role in hTF recognition[15,25], serving as a TfR recognition zone as well as an iron "carrier"[44]; whereas the N-lobe functions only as an iron "carrier" and therefore exhibits more labile and flexible tertiary structure.

In the N-lobe of both structures of Fe_NFe_C-hTF and Bi_NFe_C-hTF, together with a carbonate, Fe(III) and Bi(III) coordinate to two tyrosines (Tyr95 and Tyr188) and one tyrosine (Tyr188) in the N2-subdomain respectively (Figure 1 and S3). Unexpectedly, a tetradentate NTA is observed in the structure of Bi_NFe_C-hTF. Although it was observed previously that iron coordinated to two tyrosine ligands and a chelated nitrilotriacetate in the hen iron-(N-lobe)-ovotransferrin with an open-cleft nature, this structure was prepared by soaking crystals of the apo-protein with Fe(NTA)[45]. Involvement of only two tyrosines binding to iron was also noticed in ferric-iron binding protein (Fbp) with the protein in the opened conformation[46,47]. The present structures evidence that Tyr188 is critical for metal coordination, serving as either the initial binding contact or the last leaving residue in the metal release process, compared with other putative binding residues (Tyr95, Asp63 and His249). Very recent molecular dynamics simulations also revealed that Tyr188 is the last leaving residue for iron release[48]. Our structural work hence clearly suggests that the order of binding affinity among the four potential binding residues in N-lobe is Tyr188 > Tyr95 > His249 ≈ Asp63.

Furthermore, we found that carbonate still binds to metal even after the dissociation of the three coordinating residues Asp63, His249 and Tyr95 (Figure 1b, 1c, 1e), in contrast to the previous speculation that the carbonate should be the first leaving ligand and play an essential role in inducing protein conformational changes. We therefore proposed that during iron release process, the synergistic carbonate is associated with metal binding all the time, and the Tyr188 has a higher binding affinity to metal ions than the other three potential binding residues (Asp63, His249 and Tyr95). The disruption of coordination bonds between metal and binding residues is accompanied with protein tertiary structural change from "fully-closed" conformation to "partially-opened" and finally to "fully-opened" conformation.

The glycan moieties were also identified binding to residues Asn413 and Asn611 in the C-lobe of hTF (Figure 1 and S4), providing useful structural information on the functional studies of oligosaccharides in the protein. Although the biological advantages of conjugation of oligosaccharides to TF proteins remain unknown and the absence of carbohydrate in hTF has no effect on its recognition by TfR *in vitro*[27], the highly hydrophilic clusters of carbohydrate may alter the polarity and solubility of the proteins and abnormal glycosylation of hTF is a feature of many diseases[49], suggesting that glycan chains may involve in other important processes during the biological turnover of hTF.

In summary, we have reported the first structures of differic and bismuth bound transferrin with their N-lobes exhibiting unique "partially-opened" conformations. Only tyrosine(s) in the N2-subdomain of the N-lobe involve in metal binding, in contrast to four highly conserved binding residues in the C-lobe (Figure 1c and Table 2). Our structures of hTF represent an important conformer of the protein, providing a structural basis for understanding the mechanism of metal/metallodrug uptake and release in transferrin.

Methods

Protein purification and Fe_NFe_C-hTF preparation. Lyophilized apo-hTF was obtained from Sigma and reconstituted in 10 mM HEPES, pH 7.4 at a protein concentration of 100 mg/ml. After the incubation with 10 mM EDTA for 4 hours at room temperature, the protein was purified by gel filtration using a Superdex 200, Hiload 16/60 column on FPLC to remove the trace amount of metal ions and free anions. The apo-hTF was then concentrated by amicon to the concentration of 50 mg/ml. Upon addition of 5 mM $NaHCO_3$, the protein was incubated overnight with 4 molar equivalents of $FeNH_4(SO_4)_2$ at room temperature. Two Fe(III) ions were found binding to one hTF molecule as evidenced by the appearance of the absorption in the visible region at 465 nm. The diferric hTF (Fe_NFe_C-hTF) was further purified by gel filtration using a Superdex 200, Hiload 16/60 column on FPLC and concentrated to 30 mg/ml. The purity of proteins (apo-hTF and Fe_NFe_C-hTF) was further checked by SDS-PAGE.

Crystallization of Fe_NFe_C-hTF. The crystals used for data collection were obtained by sitting drop vapor diffusion method at 271 K. Briefly, diferric hTF at a concentration of 30 mg/ml in 10 mM HEPES pH 7.4 was mixed with an equal volume of reservoir solution composed of 10 mM HEPES pH 7.4 and 14–15% PEG 3000. Orange-red crystals appeared after 2–3 days. The crystals were cryoprotected in the solution of 10 mM HEPES pH 7.4, 30% PEG 3000 and 15% ethylene glycol and then flash-frozen in liquid nitrogen.

Soaking Bi(III) into hTF crystals. The crystals of Fe_NFe_C-hTF were pre-treated in a EDTA solution (10 mM HEPES, pH 7.4, 10 mM EDTA, 30% PEG 3000) for 3 hours at 271 K, and then transferred to a Bi(III) solution (10 mM HEPES, pH 7.4, 35% PEG 3000, 2 mM Bi(NTA)) and incubated for 3 hours at the same temperature. The crystals were selected and cryoprotected in the solution of 10 mM HEPES pH 7.4, 30% PEG 3000 and 15% ethylene glycol and then flash-frozen in liquid nitrogen.

Data collection and structure determination. Fe_NFe_C-hTF: The diffraction data were collected at 100 K at BL17U at the Shanghai Synchrotron Radiation Facility and processed with HKL2000[50]. The structure was solved by molecular replacement method with the program Phaser[51] from CCP4 suite[52] using the N-lobe of apo-hTF (PDB: 2HAV) and the C-lobe of iron bound rabbit serum transferrin (PDB: 1JNF) as search models. The model was refined with Refmac[30] implemented in CCP4 suite and then cycled with rebuilding in Coot[30]. The Fe(III), CO_3^{2-} and SO_4^{2-} as well as the NAG moieties were built into the positive electron density maps after a few round of restrained refinement. TLS refinement[53,54] was incorporated into the later stages of the refinement process. The final model was analyzed with PROCHECK[55]. Data collection and model refinement statistics are summarized in Table 1. The coordinates and structure factors were deposited in the Protein Data Bank with the code 3QYT.

Bi_NFe_C-hTF: The diffraction data were collected similarly to Fe_NFe_C-hTF and processed with HKL2000 except that the data were collected just above the L-III absorption edge of bismuth (0.92000 Å)[50]. The structure was solved by molecular replacement method with the program Phaser[52] from CCP4 suite[30] using the structure of Fe_NFe_C-hTF as a search model. The model was refined with Refmac[30] implemented in CCP4 suite and then cycled with rebuilding in Coot[53]. The Bi(III), Fe(III), CO_3^{2-}, NTA and the NAG moiety were built into the positive electron density maps after a few round of restrained refinement. TLS refinement was incorporated into the later stages of the refinement process[54,55]. Data collection and model refinement statistics are summarized in Table 1. The coordinates and structure factors were deposited in the Protein Data Bank (PDBID: 4H0W).

1. Thompson, K. H. & Orvig, C. Boon and bane of metal ions in medicine. *Science* **300**, 936–939 (2003).
2. Aisen, P. *Biological inorganic chemistry: structure and reactivity.* (University Science Books: California, 2006).
3. Qian, Z. M., Li, H., Sun, H. & Ho, K. Targeted drug delivery via the transferrin receptor-mediated endocytosis pathway. *Pharmacol Rev* **54**, 561–587 (2002).
4. Sun, H., Li, H. & Sadler, P. J. Transferrin as a metal ion mediator. *Chem Rev* **99**, 2817–2842 (1999).
5. Alexeev, D. *et al.* A novel protein-mineral interface. *Nat Struc Biol* **10**, 297–302 (2003).
6. Anderson, B. F., Baker, H. M., Norris, G. E., Rumball, S. V. & Baker, E. N. Apolactoferrin structure demonstrates ligand-induced conformational change in transferrins. *Nature* **344**, 784–787 (1990).
7. Aisen, P., Leibman, A. & Zweier, J. Stoichiometric and site characteristics of the binding of iron to human transferrin. *J Biol Chem* **253**, 1930–1937 (1978).
8. Drakesmith, H. & Prentice, A. Viral infection and iron metabolism. *Nat Rev Microbiol* **6**, 541–552 (2008).
9. Aisen, P., Enns, C. & Wessling-Resnick, M. Chemistry and biology of eukaryotic iron metabolism. *Int J Biochem Cell Biol* **33**, 940–959 (2001).
10. Halliwell, B. Free radicals, antioxidants, and human disease: curiosity, cause, or consequence? *Lancet* **344**, 721–724 (1994).
11. Campenhout, A. V., Van Campenhout, C. M., Lagrou, A. R. & Keenoy, B. M. Y. Transferrin modifications and lipid peroxidation: Implications in diabetes mellitus. *Free Radical Res* **37**, 1069–1077 (2003).
12. He, Q. M., A. B. *Molecular and cellular iron transport.* (CRC Press: New York, 2002).

13. Jensen, M. P. *et al.* An iron-dependent and transferrin-mediated cellular uptake pathway for plutonium. *Nat Chem Biol* **7**, 560–565 (2011).
14. Zhang, L. *et al.* Interactions of bismuth with human lactoferrin and recognition of the Bi(III)-lactoferrin complex by intestinal cells. *Biochemistry* **40**, 13281–13287 (2001).
15. Cheng, Y., Zak, O., Aisen, P., Harrison, S. C. & Walz, T. Structure of the human transferrin receptor-transferrin complex. *Cell* **116**, 565–576 (2004).
16. Klausner, R. D., Ashwell, G., van Renswoude, J., Harford, J. B. & Bridges, K. R. Binding of apotransferrin to K562 cells: explanation of the transferrin cycle. *Proc Natl Acad Sci USA* **80**, 2263–2266 (1983).
17. Eckenroth, B. E., Steere, A. N., Chasteen, N. D., Everse, S. J. & Mason, A. B. How the binding of human transferrin primes the transferrin receptor potentiating iron release at endosomal pH. *Proc Natl Acad Sci USA* **108**, 13089–13094 (2011).
18. Baker, E. N. Structure and reactivity of transferrins. *Advn Inorg Chem* **41**, 389–463 (1994).
19. Nguyen, S. A. K., Craig, A. & Raymond, K. N. Transferrin - the role of conformational-changes in iron removal by chelators. *J Am Chem Soc* **115**, 6758–6764 (1993).
20. Lawrence, C. M. *et al.* Crystal structure of the ectodomain of human transferrin receptor. *Science* **286**, 779–782 (1999).
21. Baker, H. M., Anderson, B. F. & Baker, E. N. Dealing with iron: common structural principles in proteins that transport iron and heme. *Proc Natl Acad Sci USA* **100**, 3579–3583 (2003).
22. Tokuriki, N. & Tawfik, D. S. Protein dynamism and evolvability. *Science* **324**, 203–207 (2009).
23. Bhabha, G. *et al.* A dynamic knockout reveals that conformational fluctuations influence the chemical step of enzyme catalysis. *Science* **332**, 234–238 (2011).
24. Beatty, E. J. *et al.* Interlobe communication in ^{13}C-methionine-labeled human transferrin. *Biochemistry* **35**, 7635–7642 (1996).
25. Gumerov, D. R., Mason, A. B. & Kaltashov, I. A. Interlobe communication in human serum transferrin: metal binding and conformational dynamics investigated by electrospray ionization mass spectrometry. *Biochemistry* **42**, 5421–5428 (2003).
26. Wally, J. *et al.* The crystal structure of iron-free human serum transferrin provides insight into inter-lobe communication and receptor binding. *J Biol Chem* **281**, 24934–24944 (2006).
27. Adams, T. E. *et al.* The position of arginine 124 controls the rate of iron release from the N-lobe of human serum transferrin. A structural study. *J Biol Chem* **278**, 6027–6033 (2003).
28. Noinaj, N. *et al.* Structural basis for iron piracy by pathogenic *Neisseria*. *Nature* **483**, 53–58 (2012).
29. Jeffrey, P. D. *et al.* Ligand-induced conformational change in transferrins: crystal structure of the open form of the N-terminal half-molecule of human transferrin. *Biochemistry* **37**, 13978–13986 (1998).
30. Emsley, P., Lohkamp, B., Scott, W. G. & Cowtan, K. Features and development of Coot. *Acta Crystallogr D* **66**, 486–501 (2010).
31. Kurokawa, H., Dewan, J. C., Mikami, B., Sacchettini, J. C. & Hirose, M. Crystal structure of hen apo-ovotransferrin. Both lobes adopt an open conformation upon loss of iron. *J Biol Chem* **274**, 28445–28452 (1999).
32. Hall, D. R. *et al.* The crystal and molecular structures of diferric porcine and rabbit serum transferrins at resolutions of 2.15 and 2.60 angstrom, respectively. *Acta Crystallogr D* **58**, 70–80 (2002).
33. Kurokawa, H., Mikami, B. & Hirose, M. Crystal structure of diferric hen ovotransferrin at 2.4 Å resolution. *J Mol Biol* **254**, 196–207 (1995).
34. Jameson, G. B., Anderson, B. F., Norris, G. E., Thomas, D. H. & Baker, E. N. Structure of human apolactoferrin at 2.0 angstrom resolution. Refinement and analysis of ligand-induced conformational change. *Acta Crystallogr D* **54**, 1319–1335 (1998).
35. Baker, H. M. *et al.* Anion binding by transferrins: Importance of second-shell effects revealed by the crystal structure of oxalate-substituted diferric lactoferrin. *Biochemistry* **35**, 9007–9013 (1996).
36. He, Q. Y., Mason, A. B., Tam, B. M., MacGillivray, R. T. A. & Woodworth, R. C. Dual role of Lys206-Lys296 interaction in human transferrin N-lobe: Iron-release trigger and anion-binding site. *Biochemistry* **38**, 9704–9711 (1999).
37. Wally, J. & Buchanan, S. K. A structural comparison of human serum transferrin and human lactoferrin. *BioMetals* **20**, 249–262 (2007).
38. Sakajiri, T., Yamamura, T., Kikuchi, T. & Yajima, H. Computational Structure Models of Apo and Diferric Transferrin-Transferrin Receptor Complexes. *Protein J* **28**, 407–414 (2009).
39. Yang, N. & Sun, H. Biocoordination chemistry of bismuth: Recent advances. *Coord Chem Rev* **251**, 2354–2366 (2007).
40. Grossmann, J. G. *et al.* The nature of ligand-induced conformational change in transferrin in solution. An investigation using X-ray scattering, XAFS and site-directed mutants. *J Mol Biol* **279**, 461–472 (1998).
41. Grossmann, J. G. *et al.* Metal-induced conformational changes in transferrins. *J Mol Biol* **229**, 585–590 (1993).
42. Ge, R. & Sun, H. Bioinorganic chemistry of bismuth and antimony: target sites of metallodrugs. *Acc Chem Res* **40**, 267–274 (2007).
43. Ge, R. *et al.* A proteomic approach for the identification of bismuth-binding proteins in *Helicobacter pylori*. *J Biol Inorg Chem* **12**, 831–842 (2007).
44. Liu, R. T., Guan, J. Q., Zak, O., Aisen, P. & Chance, M. R. Structural reorganization of the transferrin C-lobe and transferrin receptor upon complex formation: The C-lobe binds to the receptor helical domain. *Biochemistry* **42**, 12447–12454 (2003).
45. Mizutani, K., Yamashita, H., Kurokawa, H., Mikami, B. & Hirose, M. Alternative structural state of transferrin. The crystallographic analysis of iron-loaded but domain-opened ovotransferrin N-lobe. *J Biol Chem* **274**, 10190–10194 (1999).
46. Zhu, H., Alexeev, D., Hunter, D. J., Campopiano, D. J. & Sadler, P. J. Oxo-iron clusters in a bacterial iron-trafficking protein: new roles for a conserved motif. *Biochem J* **376**, 35–41 (2003).
47. Khambati, H. K. *et al.* The role of vicinal tyrosine residues in the function of *Haemophilus influenzae* ferric-binding protein A. *Biochem J* **432**, 57–64 (2010).
48. Mujika, J. I., Escribano, B., Akhmatskaya, E., Ugalde, J. M. & Lopez, X. Molecular dynamics simulations of iron- and aluminum-loaded serum transferrin: protonation of Tyr188 is necessary to prompt metal release. *Biochemistry* **51**, 7017–7027 (2012).
49. Charlwood, J., Birrell, H., Tolson, D. & Camilleri, P. Two-dimensional chromatography in the analysis of complex glycans from transferrin. *Anal Chem* **70**, 2530–2535 (1998).
50. Otwinowski, Z. & Minor, W. Processing of X-ray diffraction data collected in oscillation mode. *Methods Enzymol* **276**, 307–325 (1997).
51. Mccoy, A. J. *et al.* Phaser crystallographic software. *J Appl Crystallogr* **40**, 658–674 (2007).
52. Bailey, S. The Ccp4 Suite - Programs for protein crystallography. *Acta Crystallogr D* **50**, 760–763 (1994).
53. Painter, J. & Merritt, E. A. Optimal description of a protein structure in terms of multiple groups undergoing TLS motion. *Acta Crystallogr D* **62**, 439–450 (2006).
54. Painter, J. & Merritt, E. A. TLSMD web server for the generation of multi-group TLS models. *J Appl Crystallogr* **39**, 109–111 (2006).
55. Laskowski, R. A., Macarthur, M. W., Moss, D. S. & Thornton, J. M. Procheck - a program to check the stereochemical quality of protein structures. *J Appl Crystallogr* **26**, 283–291 (1993).

Acknowledgments

This work is supported by the Research Grants Council of Hong Kong (HKU7049/09P, *N*_HKU752/09, HKU7053/10P), Croucher Foundation and the Strategic Research Theme of the University of Hong Kong. We thank Sunney I. Chan (Caltech) for helpful comments, Stephen S.Y. Chui for crystal screening on the in-house X-ray diffractometer and the BL17U1 beam-line of the Shanghai Synchrotron Radiation Facility (SSRF) for beam time.

Author contributions

NY and HMZ carried out all the crystallography experiments. NY, HMZ, MJW, QH and HS analysed all the structural data. NY, HMZ, QH and HS wrote the manuscript. QH and HS conceived of the study, designed all experiments. All authors discussed the results, have read and approved the manuscript.

Additional information

Supplementary information accompanies this paper at http://www.nature.com/scientificreports

Competing financial interests: The authors declare no competing financial interests.

How to cite this article: Yang, N., Zhang, H., Wang, M., Hao, Q. & Sun, H. Iron and bismuth bound human serum transferrin reveals a partially-opened conformation in the N-lobe. *Sci. Rep.* **2**, 999; DOI:10.1038/srep00999 (2012).